JAAS

# Sensitive detection of trace precious metals in acidic solutions using liquid sheet jet laser-induced breakdown spectroscopy


| | |
|---|---|
| Journal: | *Journal of Analytical Atomic Spectrometry* |
| Manuscript ID | JA-TEC-12-2024-000467.R1 |
| Article Type: | Technical Note |
| Date Submitted by the Author: | 27-Mar-2025 |


| | |
|---|---|
| Complete List of Authors: | Nakanishi, Ryuzo; National Institutes for Quantum Science and Technology<br>Saeki, Morihisa; National Institutes for Quantum Science and Technology<br>Ohba, Hironori; Japan Atomic Energy Agency, Collaborative Laboratories for Advanced Decommissioning Science, Fukushima Research Institute, Sector of Fukushima Research and Development; National Institutes for Quantum Science and Technology |

# Sensitive detection of trace precious metals in acidic solutions using liquid sheet jet laser-induced breakdown spectroscopy

Ryuzo Nakanishi,*[a] Morihisa Saeki [a] and Hironori Ohba [ab]

[a]*Takasaki Institute for Advanced Quantum Science, National Institutes for Quantum and Science Technology (QST), 1233 Watanuki-machi, Takasaki, Gunma, 370-1292, Japan*

[b]*Collaborative Laboratories for Advanced Decommissioning Science (CLADS), Japan Atomic Energy Agency (JAEA), 2-4 Shirakata, Tokai, Naka, Ibaraki, 319-1195, Japan*

[*]*E-mail: nakanishi.ryuzo@qst.go.jp*

**Abstract**

Rapid in-situ analysis of precious metals in liquid has been highly desired for real-time monitoring of recovery processes. We demonstrate that laser-induced breakdown spectroscopy (LIBS) combined with a liquid sheet jet provides a sensitive technique that can directly analyze trace precious metals (Au, Pt, Pd, Ag, Rh, and Ru) in acidic aqueous solutions. A glass slit nozzle resistant to corrosive acids was employed to generate a liquid sheet jet with a thickness of tens of micrometers, which mitigated the liquid splashing inherent in the direct detection of liquid by LIBS, thereby yielding persistent luminous plasma. The optimal thickness of the sheet jet for LIBS measurement was determined as 14 μm. The LIBS spectral profiles for each analyte obtained by 532 nm laser excitation were explored to select the analytical lines for quantitative analysis. The univariate calibration curves of the analyte elements were then constructed to calculate the limit of detection (LODs) as well as other figures of merit. The LODs of Au, Pt, Pd, Ag, Rh, and Ru were estimated respectively to be 0.62, 0.97, 0.09, 0.14, 0.09, and 0.15 mg $L^{-1}$, achieving detection limits below 1 mg $L^{-1}$ and being greatly improved from conventional liquid jet LIBS. Thus, liquid sheet jet LIBS would offer a useful tool for real-time monitoring of metal recovery processes.

## 1. Introduction

Recovering and recycling precious metals has become increasingly important due to their limited supply and growing demand. The recovery processes typically involve the extraction of precious metals from aqueous solutions of dissolved waste materials. Therefore, analyzing the residual metal content in these solutions is essential for monitoring the recovery process. The analysis of liquid samples is conventionally performed using atomic absorption spectroscopy (AAS) or inductively coupled plasma (ICP) techniques. It is, however, time-consuming to repeat measurements multiple times a day because these methods are laboratory-based and require sample pre-treatment, making real-time monitoring difficult. This drives the need for a technique that facilitates rapid in-situ elemental analysis of aqueous solutions, which would greatly improve both the safety and efficiency of precious metal recovery.

Laser-induced breakdown spectroscopy (LIBS) offers an alternative approach to analyzing liquid samples.[1,2] This atomic emission spectroscopy technique has emerged as a valuable tool for elemental analysis of various sample phases (solid, liquid, and gas).[3] In LIBS measurements, a pulsed laser is focused onto the sample to generate a luminous plasma. The optical emission is then collected and spectroscopically analyzed, providing qualitative and quantitative information about the elemental composition. Its capability for rapid measurements with minimal sample pre-treatment renders LIBS a useful method for in-situ elemental analysis in various fields.[4,5]

A main challenge in applying LIBS to liquid samples lies in achieving sufficient sensitivity and reproducibility.[1,2] This difficulty arises from liquid splash and fluctuation resulting from laser ablation, which quenches the laser-induced plasma generated on the liquid samples.[6–9] To address these issues inherent in liquid LIBS measurements, a variety of sampling methods have been developed,[10] including those based on liquid-to-solid conversion[11–13] and liquid jet techniques.[14–18] In the liquid-to-solid conversion, a drop of the sample liquid is dried on appropriate substrates prior to analysis, yielding high sensitivity comparable to solid LIBS. The solid conversion method is also

advantageous when sample volume is limited, such as with biomedical specimens. In the liquid jet approach, flowing liquid samples are analyzed directly. This technique is simple and applicable to long-term monitoring of temporal changes in the concentration of target elements. It is also worth noting that the LIBS signal can be accumulated without requiring mechanical adjustments of the irradiation spot until satisfactory spectral quality is obtained because each laser pulse interacts with a fresh sample surface.

Previous studies on the detection of precious metals in solution by LIBS have primarily employed the liquid-solid conversion, with only a few examples focusing on direct liquid analysis.[19] Liquid jet LIBS was used to detect Pt,[20] Pd,[21] and Ag[22,23] in liquids. UV-IR double pulse LIBS applied to a flowing bulk liquid demonstrated the detection of Au in aqueous solutions.[24] These studies reported limits of detection (LODs) ranging from a few to several tens of mg $L^{-1}$. More recently, microwave-assisted LIBS combined with a liquid jet was performed to detect Ru in solution, achieving detection limits below 1 mg $L^{-1}$.[25]

We have recently shown that LIBS using a liquid sheet jet with 10 – 20 μm thickness produces more intense plasma emission compared to the conventional cylindrical laminar jet.[26–28] The use of the liquid sheet jet suppresses splashing during plasma generation, resulting in persistent optical emissions. The LOD of Na in an aqueous solution achieved the sub-μg $L^{-1}$ range with single pulse LIBS.[28] We have further applied liquid sheet jet LIBS to the detection of Zr in water,[27] highlighting the capability of this method to detect trace heavy metals in aqueous solutions.

The present work investigates the application of liquid sheet jet LIBS for detecting precious metals (Au, Pt, Pd, Ru, Rh, and Ag) in acidic solutions. Our previous work utilized stainless steel nozzles, designed originally for dye laser applications, to generate a liquid sheet jet.[26] However, in most industrial recovery processes, precious metals are leached from waste materials using highly acidic solutions, presenting a challenge for direct liquid analysis due to corrosion damage to metal components in the analytical system. To enable LIBS analysis of these corrosive solutions without

pretreatment, we developed a glass slit nozzle to generate liquid sheet jets, overcoming metal component corrosion issues. Using this new setup, we acquired LIBS spectra via direct excitation of acidic liquid samples and identified analytical emission lines for quantitative analysis. Univariate calibration curves were then constructed to determine figures of merit. This work aims to demonstrate the potential of liquid sheet jet LIBS as a viable alternative to detect trace precious metals in acidic solutions and to lay the groundwork for in situ analysis of aqueous solutions during metal recovery processes. Our approach enables direct detection of all six precious metals in acidic solutions with detection limits below 1 mg $L^{-1}$, demonstrating improved performance over conventional liquid LIBS methods.

## 2. Experimental

The experimental setup used in this study is similar to that in our previous work.[28] Briefly, the apparatus consists of a liquid recirculation system, a Q-switched Nd:YAG laser (Continuum, PL8000), and a 0.3-meter Czerny-Turner spectrometer (Acton Research, Spectra Pro 2300i). A schematic of the experimental setup is illustrated in Fig 1(a). The liquid recirculation was performed using a peristaltic pump (Masterflex, 7559-00) with thermoplastic elastomer tubes (Masterflex, C-flex L/S16). An all-plastic syringe with a 6 mL capacity was inserted into the circuit as a pulse dampener.[29] A sample solution of 30 mL was found to be sufficient for the LIBS measurements. The sample solutions pumped from reservoirs were delivered to a glass slit nozzle at a flow rate of

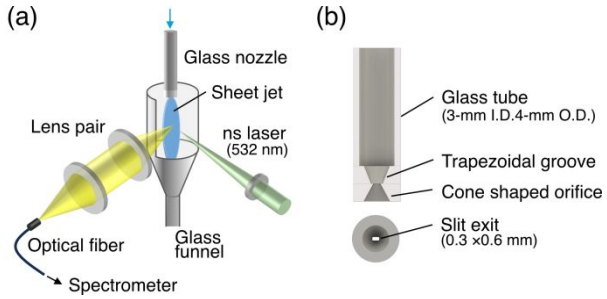


**Fig. 1** (a) Schematic illustration of experimental setup. (b) Cross-sectional view of glass nozzle and top view of slit exit.

~110 mL $min^{-1}$. The design of the nozzle was based on the stainless steel nozzle employed in our previous studies.[26,28] The nozzle is composed of a glass tube (O.D. 4 mm and I.D. 3 mm), a nozzle tip, and a cone-shaped orifice (Fig. 1(b)). The nozzle tip has a trapezoidal groove forming a single converging channel[30] with a slit exit of 0.3 × 0.6 mm. These components were connected by optical contact bonding. The nozzle was placed on a translation and rotation stage to adjust the position of the sheet jet to maximize the detected plasma emission. The sample solutions were prepared as single-element specimens diluted from ICP standard solutions of each target element (1000 mg $L^{-1}$, FUJIFILM Wako Pure Chemical Corporation). The solutions of Au, Pt, and Rh were diluted with 5 wt% (1.4 mol $L^{-1}$) HCl, and those of Ag, Pd, and Ru with 5 wt% (0.8 mol $L^{-1}$) $HNO_3$. The second harmonic output of the Nd:YAG laser (532 nm) was employed to generate plasma on the liquid sheet jet. The laser was operated at a repetition rate of 10 Hz with a pulse duration of 9 ns. The laser beam with a diameter of 9 mm was focused onto the surface of the sheet jet by a plano-convex lens with a focal length of 100 mm. The focused point was adjusted so that air breakdown takes place near the surface of the jet, where the laser-induced plasma interacts with the sample solutions. Optical emission from the plasma was collected through a pair of plano-convex lenses and introduced into an optical fiber. The collection lenses with focal lengths of 70 mm and 100 mm were placed at right angles to the laser beam. The emission light was fed into the spectrometer through the fiber, dispersed by a 1200-grooves/mm grating, and detected by an intensified charge-coupled device (ICCD) camera (Andor, iStar).

## 3. Result and discussion

### 3.1. Liquid sheet jet from glass nozzle

Figure 2(a) shows a photograph of a liquid sheet jet produced from distilled water jetting out of the glass slit nozzle. The sheet jet is composed of orthogonal leaf-shaped sheets enclosed with thick cylindrical rims in a chain-like arrangement. The thickness of the primary sheet was measured along

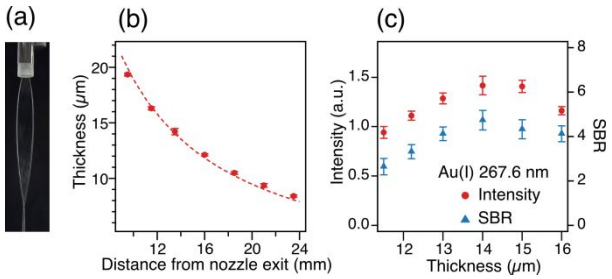


**Fig. 2** (a) Photograph of a liquid sheet jet of distilled water. (b)Sheet thickness variation with distance from nozzle exit. (c) Signal intensity and SBR for Au(I) 267.6nm line as a function of sheet thickness.

its vertical centerline using thin-film interferometry.[26] White light from a halogen lamp was focused on the surface of the liquid sheet, and fringe patterns in the reflection spectra were analyzed. As shown in Fig. 2(b), a liquid sheet with a thickness of 10 – 20 μm was generated at 10 – 20 mm from the nozzle exit. The thickness decreased inversely proportional to the distance from the exit. This is consistent with previous studies on liquid sheet jets from converging nozzles[26,30,31]. The sheet thickness, $h$, follows the expression $h = cA/x$, where $c$ is a dimensionless constant, $A$ is the area of the nozzle exit, and $x$ is the distance from the exit. The constant $c$ is determined by the aspect ratio and converging angle of a nozzle exit.[30] Consequently, the sheet thickness at a given point spot depends only on the geometrical parameters of the nozzle. This indicates that the flow rate and thermophysical properties of the liquid (i.e., density, surface tension, viscosity) hardly affect the thickness, but instead determine the width and length of the sheets.[30] Thus, the sheet thickness at a given spot remains nearly constant, even when the flow rate fluctuates or drifts, or when using liquid samples with varying metal concentrations and compositions. These features are preferable to LIBS measurements, ensuring that measurements can be conducted under consistent conditions for different samples.

The optimal thickness of the sheet jet for LIBS measurements was examined. Figure 2(c) illustrates the trends of LIBS intensities and signal-to-background ratios (SBRs) for the Au(I) 267.6 nm line as a function of the sheet thickness. The SBRs were calculated as the ratio of the background-subtracted peak height to the background intensity, providing a measure of spectral

line quality for analytical line selection. The sample solution was a 50 mg $L^{-1}$ Au in HCl and the data were measured using a laser energy of 50 mJ $pulse^{-1}$, with a gate delay of 7 µs and a gate width of 20 µs. Each data point represents the average of five repeated measurements of 30 laser shot accumulations. The spectral intensities and SBRs reached their maximum at a thickness of 14 µm, with the corresponding spot located 13.5 mm from the nozzle exit. The data presented hereafter were measured employing this laser irradiation position. This optimal thickness in the present experimental conditions is consistent with our previous finding that a thickness of 10 – 20 µm was optimal for Zr detection in aqueous solutions using 1064 nm excitation.[27]

### 3.2. LIBS Spectra of precious metals in solutions

Figure 3 summarizes typical LIBS spectra obtained from a liquid sheet jet of sample solutions containing each element. Each spectrum was accumulated over 100 laser shots. Characteristic

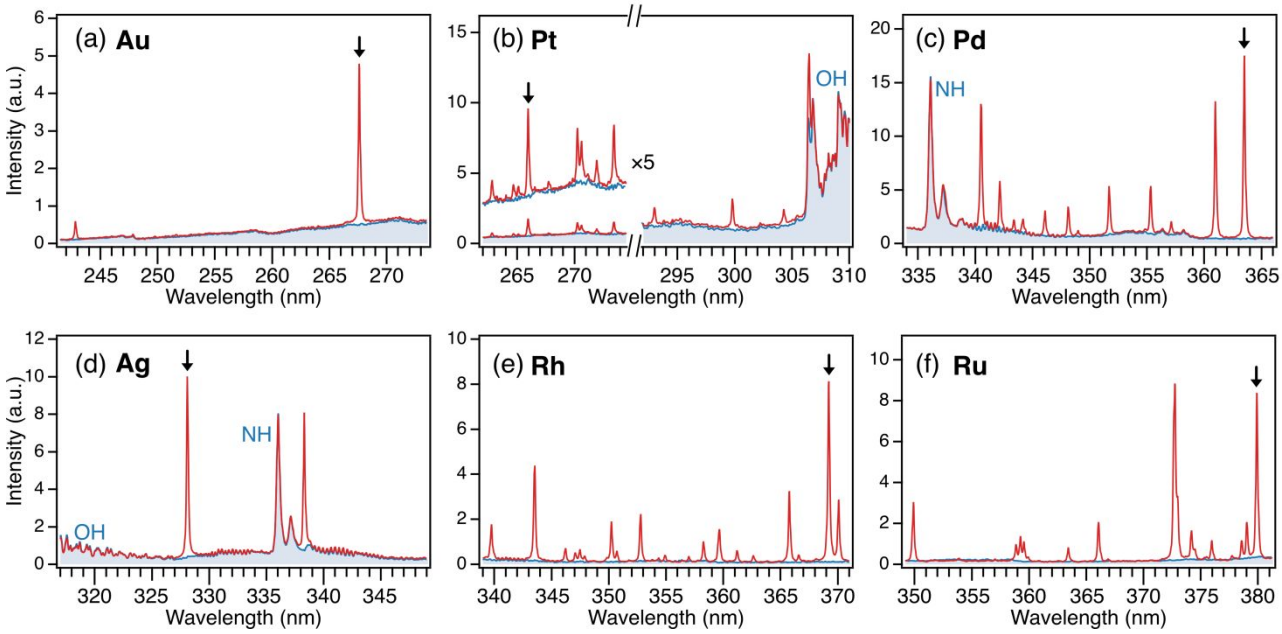


**Fig. 3** LIBS spectra of analyte elements in acidic solutions. Blue-shaded spectra represent those recorded for corresponding blank samples. (a) Au 100 mg $L^{-1}$ in 5 wt% HCl, (b) Pt 100 mg $L^{-1}$ in 5 wt% HCl, (c) Pd 50 mg $L^{-1}$ in 5 wt% $HNO_3$, (d) Ag 50 mg $L^{-1}$ in 5 wt% $HNO_3$, (e) Rh 50 mg $L^{-1}$ in 5 wt% HCl, (f) Ru 50 mg $L^{-1}$ in 5 wt% $HNO_3$. Gate delay time for Au and Pt: 5 µs, for the others: 15 µs. Gate width: 20 µs.

**Table 1** Analytical lines and experimental parameters

| Analyte element | Wavelength (nm) | $E_{upper}$ (eV) | $E_{lower}$ (eV) | Gate delay (μs) | Gate width (μs) |
|---|---|---|---|---|---|
| Au(I) | 267.6 | 4.63 | 0.00 | 6 | 6 |
| Pt(I) | 265.9 | 4.66 | 0.00 | 7 | 8 |
| Pd(I) | 363.5 | 4.22 | 0.81 | 17 | 10 |
| Ag(I) | 338.3 | 3.66 | 0.00 | 15 | 10 |
| Rh(I) | 369.2 | 3.36 | 0.00 | 17 | 10 |
| Ru(I) | 379.9 | 3.26 | 0.00 | 17 | 10 |

atomic lines of the target elements are clearly observed in the UV region. Some lines are interfered with molecular emission bands of NH, OH, and CN originating from water and ambient air,[32] which is inherent to LIBS with directly measuring liquids. Note that NH emission lines arise predominantly from ambient air, not from the $HNO_3$ solution; the NH spectral intensities remained almost the same for both distilled water and nitric acid, as observed in previous work.[27]

A cursory inspection of the LIBS spectra led us to identify the relevant spectral lines to build univariate calibration curves for each element. The selection of the lines was guided by the need to minimize interference from the molecular emission lines mentioned above. The selected lines are indicated as arrows in the spectra in Fig. 3 and listed in Table. 1 along with their energy levels.[33] For Au (Fig. 3(a)), two lines at 242.8 and 267.6 nm are visible above the background continuum emission. The 267.6 nm line is more intense, being suitable for an analytical line. From the Pt solution, several emission lines appeared in the 260 – 310 nm range (Fig.3(b)). Although the 306.5 nm line was most intense, a strong emission from OH radical (A-X) interfered, complicating the analysis of this line. The alternative candidates for the Pt analytical line are the 299.8 nm and 265.9 nm lines. As discussed later, the 265.9 nm line yielded better SBR than the 299.8 nm line, because the latter emerged on the higher background. Note that the emission intensities for Au and Pt appear weaker than the other elements due to the higher excitation energies (Table 1). The Pd sample solution exhibited several intense non-resonant lines in the 335 – 365 nm range (Fig. 3(c)), but many appeared on the NH or CN emission bands. The 363.5 nm line was among the highest and

avoided the overlap with these molecular bands. For Ag, two prominent lines were observed at 328.1 and 338.3 nm (Fig. 3(d)), both of which are resonant lines. The 328.1 nm line is located between NH and OH progression bands, while the 338.3 nm line overlaps with NH emission lines; the former is selected as a favorable analytical line. Several Rh lines appeared in the 340–370 nm range (Fig. 3(e)); the most intense emission was the 369.2 nm line. For Ru, intense lines were identified in 350 – 380 nm. The two comparable strong lines appeared at 373 and 379 nm. The former is overlapped lines of 372.7 and 372.8 nm. Therefore, we chose the 379.9 nm line as an analytical line, while slightly overlapping with the onset of the CN molecular emission band.

The experimental parameters such as laser pulse energy, gate delay, and gate width were determined to yield the best SBR of the above analytical lines for each target element to build calibration curves. We initially investigated SBRs of the Pt(I) emission lines, which yielded the weakest signals among the target elements, to determine the laser energy to be used in the subsequent LIBS measurements. The gate width was kept at 20 µs, which was sufficient to provide

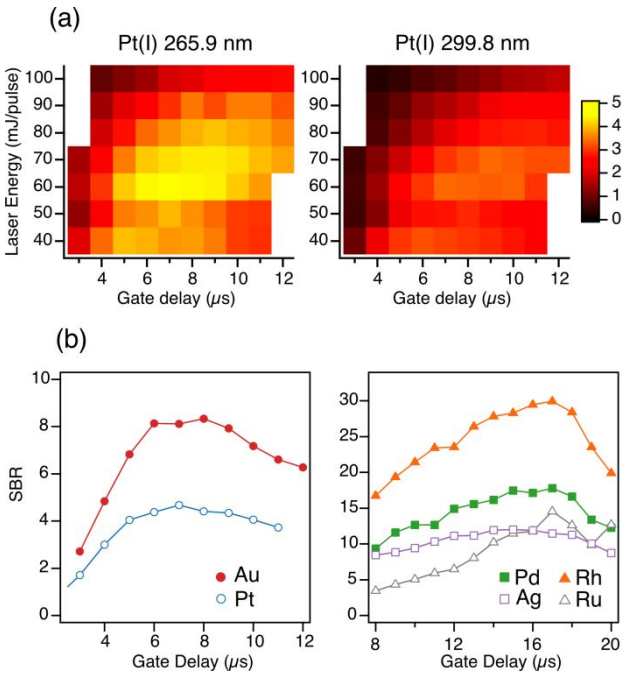


**Fig. 4** (a) SBR contour maps for Pt(I) lines (265.9 nm, 299.8 nm) obtained from LIBS spectra of Pt solution (100 mg $L^{-1}$) as a function of gate delay and laser energy. (b) SBR variation with gate delay for each element. Laser energy: 60 mJ $pulse^{-1}$; Gate width: 20 µs; Au: 60 mg $L^{-1}$; Pt: 100 mg $L^{-1}$; Pd, Ag, Rh, Ru: 20 mg $L^{-1}$.

time-integrated spectra. Figure 4(a) illustrates contour plots of SBRs of the Pt emission lines at 265.9 nm and 299.8 nm as a function of laser pulse energy and gate delay. The data were recorded for an aqueous solution of Pt (100 mg $L^{-1}$). The contours reveal that the 265.9 nm line generally shows greater SBR than the 299.8 nm line for the experimental conditions investigated here and that SBRs for those lines reach the maximum value at a laser energy of 60 mJ $pulse^{-1}$ and a gate delay time of 7 μs. The best gate delays for the other elements were subsequently determined with the laser energy maintained at 60 mJ $pulse^{-1}$. Figure 4(b) shows the SBR variations with gate delay for each element. Due to the weaker signals for Pt and Au emission lines on the higher continuum background, the optimal gate delays for those elements were shorter than the other elements (Ag, Pd, Rh, Ru). The SBRs for the emission lines of Pt and Au reached their maximum values at delay times of 6 – 8 μs, while those for the other elements exhibited maxima at delay times longer than 15 μs (Fig. 4(b)). The determined gate delays are included in Table 1. These values for the acquisition gate delay time are much longer than those for other direct liquid LIBS measurements (0.5 – 5 μs),[20–24] suggesting a longer lifetime for the laser-induced plasma generated on the liquid-sheet jet. The longer plasma lifetime is attributable to reduced liquid splash, a primary factor in plasma quenching for liquid LIBS. Our previous work has revealed that the laser-induced plasma on the thin liquid sheet avoids splashing on the front surface; the irradiation of the laser pulse perforates the thin sheet, generating a hole that prevents further splashing.[28] This contrasts with conventional liquid LIBS configurations, where substantial splashing occurs on the front surfaces of the liquid sample. The SBRs with different gate widths were also investigated at the fixed laser energy and the gate delays determined above. Although the SBR values were much less susceptible to the gate widths, the optimal values were determined as the shortest times at which they reached their maxima. The determined gate widths are also included in Table 1.

### 3.3. Calibration curves

To assess the sensitivity of liquid sheet-jet LIBS, univariate calibration curves were established for the target elements based on the peak height intensities of the analytical lines (Table 1) obtained under the experimental conditions determined above. Figure 5 presents the calibration curves of the analyte elements. The concentration ranges of Au and Pt were 0 – 60 mg $L^{-1}$ and those of the other elements were 0 – 20 mg $L^{-1}$. The intensity data were obtained by averaging five repeated measurements, with each accumulated over 400 laser shots. Different accumulation parameters were used for parameter optimization (30 shots) and calibration measurements to balance efficiency and accuracy requirements. The increased accumulation for the calibration measurements resulted in spectral relative standard deviations (RSDs) of approximately 2% for the highest concentration samples, thereby increasing the reliability of the calculated figures of merit. The linear fitting results show good linearity without indication of self-absorption within the investigated concentration ranges; the coefficient determinations, $R^2$, are greater than 0.998 for all the elements. The LODs were then calculated using the conventional formula of $3\sigma/S$, where $\sigma$ represents the standard deviation of the blank signal, and $S$ is the slope of the fitted curves. The LOD values thus determined are listed in Table 2 along with $R^2$, RSD, root mean square error of calibration (RMSEC), and mean relative error (MRE) derived from the calibration data. The LODs of Au and Pt are 0.62 and 0.97 mg $L^{-1}$, and those of Pd, Ag, Rh, and Ru are as low as 0.09, 0.14, 0.09, and 0.15 mg $L^{-1}$, respectively. The present study achieves detection limits below 1 mg $L^{-1}$ and exhibits a notable improvement compared with the reported LODs for direct liquid LIBS: Au (13.5 mg $L^{-1}$)[24], Pt (90 mg $L^{-1}$)[20], Ag (3.1 mg $L^{-1}$)[22], and Ru (0.957 mg $L^{-1}$).[25] To our knowledge, this work presents the first direct liquid LIBS detection of Pd and Rh

**Table 2** $R^2$, RSD, RMSEC, MRE, and LOD of analyte elements

| Analyte element | $R^2$ | RSD (%) | RMSEC (mg $L^{-1}$) | MRE (%) | LOD (mg $L^{-1}$) | |
|---|---|---|---|---|---|---|
| | | | | | this work | literature |
| Au | 0.999 | 6.1 | 0.44 | 4.3 | 0.62 | 13.5 (ref. 24) |
| Pt | 0.998 | 10.2 | 0.89 | 6.3 | 0.97 | 90 (ref. 20) |
| Pd | 0.999 | 12.0 | 0.17 | 12.0 | 0.09 | – |
| Ag | 0.998 | 11.6 | 0.24 | 11.4 | 0.14 | 3.1 (ref. 22) |
| Rh | 0.999 | 7.8 | 0.17 | 6.0 | 0.09 | – |
| Ru | 0.998 | 12.3 | 0.30 | 9.0 | 0.15 | 0.957 (ref. 25) |

in solution. A direct comparison with measurement stability from previous studies is difficult due to the limited precision metrics reported in the literature; however, given that our RSD value is comparable to the 10% RSD reported in the literature,[20] the detection limits were improved without sacrificing the reproducibility of the measurements. These findings demonstrated that direct liquid LIBS combined with a liquid sheet jet proved an effective method for detecting trace amounts of precious metal elements in acidic solutions.

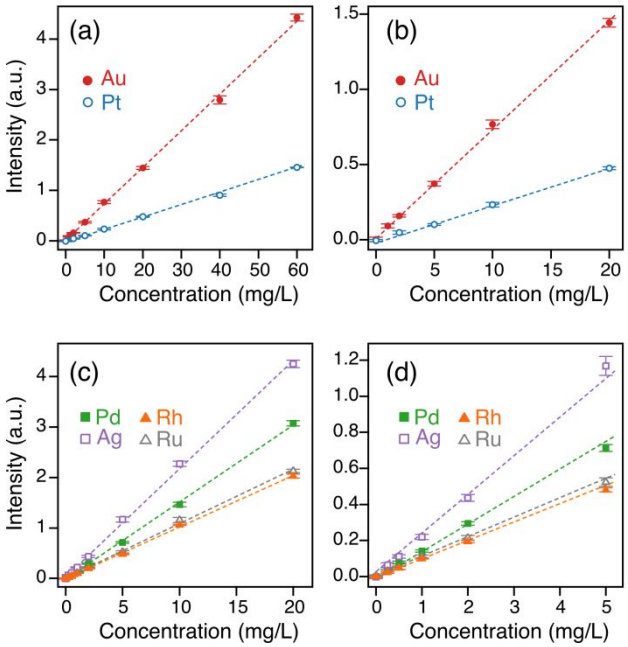


**Fig. 5** (a)(c) Calibration curves for each analyte element. (b)(d) Expanded views of lower concentration region.

## 4. Conclusions

We have demonstrated the capability of liquid sheet jet LIBS for sensitive detection of precious metals (Au, Pt, Pd, Ag, Rh, and Ru) in acidic solutions via direct liquid analysis. A liquid sheet with a thickness of several tens of micrometers was formed by using a newly fabricated glass slit nozzle resistant to corrosive acidic solutions. By focusing a 532 nm laser pulse onto a spot with a thickness of 14 μm, luminous laser-induced plasma was generated on the surface of the jet at ambient pressure and temperature. The emission lines of each analyte were clearly identified. Among these, the lines with high intensity, high SBR, and minimal interference with background signals from air and water were selected for quantitative analysis. Linear calibration curves were established based on these analytical lines, exhibiting excellent linearity and achieving the LODs below 1 mg $L^{-1}$ for all the elements analyzed in this study. The obtained LODs of Au, Pt, Ag, and Ru are appreciably improved compared to previously reported values for direct liquid LIBS, while the LODs of Pd and Rh in direct liquid analysis are reported here for the first time. Notably, this work introduces the acid-resistant system for liquid sheet jet LIBS, enabling direct analysis of precious metals in their acidic media with enhanced sensitivity compared to previous direct liquid methods. Although this preliminary study focused on the simple systems involving single-element standard solutions with univariate analysis, the present findings highlight the potential and the applicability of the liquid sheet jet LIBS methodology for detecting trace levels of precious metals in aqueous solutions and monitoring their temporal evolution during recovery processes. For practical applications, the substantial variation in optimal gate delay among the elements (Table 1) introduces a challenge for multi-element detection. Addressing this challenge may involve either selecting a compromise gate delay or performing sequential measurements with element-specific parameters. Research for multi-element analysis using liquid sheet jet LIBS is underway, specifically assessing the techniques to handle the complexity encountered in actual recovery process solutions.

## Author contributions

Ryuzo Nakanishi: methodology, experiments, data analysis, original draft, and writing of the manuscript. Morihisa Saeki, Hironori Ohba: methodology, reviewing and editing of the manuscript.

## Conflicts of interest

There are no conflicts to declare.

## Data availability

The data supporting the results presented in this paper are available from the corresponding author upon reasonable request.

## Acknowledgments

This work was supported by JSPS KAKENHI Grant Number JP24K00622 and Adaptable and Seamless Technology transfer Program through Target-driven R&D (A-STEP) from Japan Science and Technology Agency (JST) Grant Number JPMJTM20KV.

## References

1 K. Keerthi, S. D. George, S. D. Kulkarni, S. Chidangil and V. K. Unnikrishnan, *Opt. Laser Technol.*, 2022, **147**, 107622.

2 I. Goncharova, D. Guichaoua, S. Taboukhat, A. Tarbi, T. Chtouki, H. Erguig and B. Sahraoui, *Spectrochim. Acta Part B*, 2024, **217**, 106943.

3 D. A. Cremers and L. J. Radziemski, *Handbook of Laser-Induced Breakdown Spectroscopy*, John Wiley & Sons, 2013.

4 F. J. Fortes, J. Moros, P. Lucena, L. M. Cabalín and J. J. Laserna, *Anal. Chem.*, 2013, **85**, 640.

5 X. Yu, Y. Li, X. Gu, J. Bao, H. Yang and L. Sun, *Environ. Monit. Assess.*, 2014, **186**, 8969.

6 D. A. Cremers, L. J. Radziemski and T. R. Loree, *Appl. Spectrosc.*, 1984, **38**, 721.

7 B. Charfi and M. A. Harith, *Spectrochim. Acta Part B*, 2002, **57**, 1141.

8 A. De Giacomo, M. Dell'Aglio and O. De Pascale, *Appl. Phys. A*, 2004, **79**, 1035.

9 V. Lazic and S. Jovićević, *Spectrochim. Acta Part B*, 2014, **101**, 288.

10 K. Keerthi, S. D. George, J. G. Sebastian, A. K. Warrier, S. Chidangil and V. K. Unnikrishnan, *J. Anal. At. Spectrom.*, 2022, **37**, 2625.

11 T. Ohta, M. Ito, T. Kotani and T. Hattori, *Appl. Spectrosc.*, 2009, **63**, 555.

12 M. A. Aguirre, S. Legnaioli, F. Almodóvar, M. Hidalgo, V. Palleschi and A. Canals, *Spectrochim. Acta Part B*, 2013, **79-80**, 88.

13 A. De Giacomo, C. Koral, G. Valenza, R. Gaudiuso and M. Dell'Aglio, *Anal. Chem.*, 2016, **88**, 5251.

14 Y. Ito, O. Ueki and S. Nakamura, *Anal. Chim. Acta*, 1995, **299**, 401.

15 F.-Y. Yueh, R. C. Sharma, J. P. Singh, H. Zhang and W. A. Spencer, *J. Air Waste Manage. Assoc.*, 2002, **52**, 1307.

16 Y. Feng, J. Yang, J. Fan, G. Yao, X. Ji, X. Zhang, X. Zheng and Z. Cui, *Appl. Opt.*, 2010, **49**, C70.

17 D. C. Zhang, Z. Q. Hu, Y. B. Su, B. Hai, X. L. Zhu, J. F. Zhu and X. Ma, *Opt. Express*, 2018, **26**, 18794.

18 D. Zhang, R. Yang, H. Ge, Z. Feng, G. Wang, J. Hou, W. Tian and J. Zhu, *Spectrochim. Acta Part B*, 2023, **204**, 106670.

19 N. Schlatter and B. G. Lottermoser, *Spectrosc. J.*, 2024, **2**, 1.

20 F. A. Barreda, F. Trichard, S. Barbier, N. Gilon and L. Saint-Jalmes, *Anal. Bioanal. Chem.*, 2012, **403**, 2601.

21 S. C. Snyder, W. G. Wickun, J. M. Mode, B. D. Gurney and F. G. Michels, *Appl. Spectrosc.*,

2011, **65**, 642.

22 P. Yaroshchyk, R. J. S. Morrison, D. Body and B. L. Chadwick, *Spectrochim. Acta Part B*, 2005, **60**, 986.

23 P. Fichet, M. Tabarant, B. Salle and C. Gautier, *Anal. Bioanal. Chem.*, 2006, **385**, 338.

24 K. Rifai, S. Laville, F. Vidal, M. Sabsabi and M. Chaker, *J. Anal. At. Spectrom.*, 2012, **27**, 276.

25 A. F. A. Kasim, M. A. Wakil, K. Grant, M. Hearn and Z. T Alwahabi, *Plasma Sci. Technol.*, 2022, **24**, 084004.

26 H. Ohba, M. Saeki, I. Wakaida, R. Tanabe and Y. Ito, *Opt. Express*, 2014, **22**, 24478.

27 A. Ruas, A. Matsumoto, H. Ohba, K. Akaoka and I. Wakaida, *Spectrochim. Acta Part B*, 2017, **131**, 99.

28 R. Nakanishi, H. Ohba, M. Saeki, I. Wakaida, R. Tanabe-Yamagishi and Y. Ito, *Opt. Express*, 2021, **29**, 5205.

29 A. Picchiotti, V. I. Prokhorenko and R. J. Miller, *Rev. Sci. Instrum.*, 2015, **86**, 093105.

30 B. Ha, D. P. DePonte and J. G. Santiago, *Phys. Rev. Fluids*, 2018, **3**, 114202.

31 C. J. Crissman, M. Mo, Z. Chen, J. Yang, D. A. Huyke, S. H. Glenzer, K. Ledbetter, J. P. F Nunes, M. L. Ng, H. Wang, X. Shen, X. Wang and D. P. DePonte, *Lab Chip*, 2022, **22**, 1365.

32 G. Dinescu, E. Aldea, M. L. De Giorgi, A. Luches, A. Perrone and A. Zocco, *Appl. Surf. Sci.*, 1998, **127**, 697.

33 A. Kramida, Y. Ralchenko, J. Reader and NIST ASD Team, *NIST Atomic Spectra Database (ver. 5.12),* Online, https://physics.nist.gov/asd (accessed November 2024).

## Data Availability Statement

The data supporting the results presented in this paper are available from the corresponding author upon reasonable request.